Journal of Arid Environments 176 (2020) 104120

Contents lists available at ScienceDirect

Journal of Arid Environments

journal homepage: www.elsevier.com/locate/jaridenv

A mechanistic investigation of the oasis effect in the Zhangye cropland in semiarid western China

Sophie Ruehr[a,*], Xuhui Lee[a], Ronald Smith[b], Xin Li[c], Ziwei Xu[d], Shaomin Liu[d], Xiaofan Yang[d], Yanzhao Zhou[c]

[a] School of Forestry & Environmental Studies, Yale University, New Haven, CT, 06511, USA
[b] Department of Geology & Geophysics, Yale University, New Haven, CT, 06520, USA
[c] Institute of Tibetan Plateau Research, Chinese Academy of Sciences, Beijing, USA
[d] State Key Laboratory of Earth Surface Processes and Resource Ecology, Faculty of Geographical Science, Beijing Normal University, Beijing, 100875, China

ARTICLE INFO

Keywords:
Oasis-desert system
Energy balance
Intrinsic biophysical mechanism (IBPM)
Semi-arid region

ABSTRACT

Providing mechanistic explanations for oasis cold island effect trends expands current understanding of how land use change affects local climate in semi-arid regions globally. Data from Zhangye, Gansu, China in 2013 were used to evaluate intrinsic biophysical mechanism (IBPM) theory's ability to model the oasis effect. The land-surface temperature oasis effect is observed most intensely in summer afternoon (average difference -12.66 ± 6.6 K at 13:30 between oasis and desert sites). Observed land-surface temperature oasis effects result from differences in surface albedo, Bowen ratio, soil heat flux and air temperature. The Bowen ratio change is the strongest predictor of land-surface temperature oasis effect, with a nearly 1:1 relationship to the observed land-surface oasis effect in summer ($R^2 = 0.6$). The IBPM theory accurately predicts oasis effects for 66% of summer daylight hours, with an average RSME of 4.72 K. Correlation analysis is performed to evaluate the impacts of meteorological conditions on observed oasis effects, showing that higher windspeed and greater atmospheric clarity produce stronger land-surface temperature oasis effects. In summer, this relationship is strongest, with an R^2 value of 0.65 and RSME of 3.77. This research has implications for evaluating temperature impacts of land use change in semi-arid regions globally.

1. Introduction

Increasing demand for fresh water in semi-arid and arid regions has resulted in ecological degradation and lack of access to fresh water globally, especially in recent years with population growth and expanding agricultural lands (Cheng et al., 2014; Nicholson, 2015; Li et al., 2016). As Huang et al. (2017) show, arid regions and drylands around the world face greater risks than other regions from global warming, as arid regions will likely experience greater gains in temperature than humid regions. Global dryland surface warming has been 20–40% higher than humid land surface warming over the past century. If current trends continue, arid regions may face a future of decreasing crop yields and runoff as well as increasing drought and transmission of infectious disease. Drylands represent 41% of the global terrestrial surface area (Yukie and Otto, 2011), and arid regions are expected to expand to up to 50% of the global land area by the end of this century (Huang et al., 2016). With climate change and economic development, sustainable water management and agriculture in arid and semi-arid regions is more important now than ever (Micklin, 1988; Eziz et al., 2010; Li et al., 2016; Hao et al., 2016). Despite their small footprint, oases are crucial resources of water in arid regions. In China, oases support 95% of people living in arid and semi-arid regions even though oases make up less than 5% of China's total arid land area (Li et al., 2016).

Land use change in arid regions can result in significant impacts on local climate, and boundary-layer meteorology provides useful mechanistic explanations for observed phenomena resulting from land use change. This study investigates one such phenomenon, the oasis effect, which in the "space-for-time" framework can be viewed as a climatic consequence of conversion of semiarid and arid natural land to irrigated cropland, and attempts to quantify the effect using data from Zhangye, Gansu, China, a city in a semi-arid region that is surrounded by artificial oases (agricultural fields) watered by the Heihe River via irrigation canals.

The oasis effect is defined as the difference in temperature between the oasis and surrounding desert. Often, temperatures are lower in the

* Corresponding author. Yale University, School of Forestry & Environmental Science, 195 Prospect Street, New Haven, CT, 06511, USA.
E-mail address: sophie.ruehr@aya.yale.edu (S. Ruehr).

https://doi.org/10.1016/j.jaridenv.2020.104120
Received 10 June 2019; Received in revised form 24 December 2019; Accepted 21 January 2020
0140-1963/

oases than the desert. Previous study has revealed underlying mechanisms that contribute to observed oasis effects, as well as meteorological trends correlated with the effect. Generally, the oasis effect is produced by cropland evaporative cooling (Kai et al., 1997; Mahmood et al., 2004; Potchter et al., 2008; Douglas et al., 2009; Hao and Li, 2016). As wet, cold air moves from the oasis outwards into the dryland, intense vertical convection produces a mesoscale low-pressure system. The warm, dry air rising from the dryland moves above the oasis, creating a stable mesoclimate that reinforces the surface cooling in the oasis and a net flux of water vapor from the oasis into the dryland (Liu et al., 2007; Li et al., 2016).

Global climate modelling studies have shown that irrigation can produce temperature depressions and counteract greenhouse gas emission warming on a local level (Lobell et al., 2006; Kueppers et al., 2007; Douglas et al., 2009). Kueppers et al. (2007) used a regional climate model to compute the difference between two 20-year simulations of model and potential vegetation in California. They found that irrigation produced a significant cooling effect on average mean and maximum temperatures during the growing season (June to October), with a maximum temperature depression of -7.5 ± 0.4 K in August. Differences in winter temperature due to irrigation were negligible. Jiang et al. (2014) showed that irrigation leads to an increase in latent heat flux and decrease in sensible heat flux of 12 and 9 W m^{-2}, respectively, in northern China. They also found that irrigation expansion produces a regional cooling effect of 1.7 K on annual mean temperature. Lobell et al. (2006) found that, although irrigation did not have a significant effect on global temperatures, regional temperature depressions from irrigation counteracted greenhouse warming by up to 1 K in Europe and India.

Other studies have used meteorological and satellite data to describe the oasis effect in northwest China. Using surface energy balance to provide a mechanistic explanation for the observed effect, Kai et al. (1997) showed that the air temperature oasis effect in Zhangye results from intense latent heat flux at the oasis. They also observed a -7 K air temperature (recorded at 1 m above the surface) oasis effect in the afternoon, as well as a temperature inversion over the oasis, resulting in a negative (downward) sensible heat flux and large positive (upward) latent heat flux. Fang (2019) used MODIS satellite data to quantify oasis effect trends in Zhangye and found that irrigation created a -10 to -13 K daytime temperature depression during the growing season from 2001 to 2015. Nighttime oasis effects were much smaller in scale, ranging from -2 K to 2 K, over the study's period. Hao and Li (2016) used MODIS data form the Tarim Basin in northwest China to study diurnal and seasonal patterns of the oasis effect, showing that oases may exhibit heat island effects at night. Hao et al. (2016) found that the oasis effect in the Tarim Basin is greatest in summer (with an average -9.1 K gradient between oases and desert sites) with a large latent heat flux over the oasis due to increased irrigation and therefore water availability. Other studies have also considered energy balance closure in the Heihe River basin with data from sites used in this study (Song et al., 2016; Xu et al., 2017; Zhou and Li, 2019).

Meteorological conditions have been shown to influence the magnitude of the oasis effect. Potchter et al. (2008) focused on the influence of synoptic conditions on the intensity of the surface temperature oasis effect in an Israeli oasis system, concluding that higher wind velocity and greater relative humidity decreased the oasis effect. Taha et al. (1991) studied how temperature varies with meteorological variables within a canopy, concluding that clear days and weaker winds produce larger temperature depressions (up to 0.8 K) within the canopy. Recent studies have also investigated long-term climatic changes in northeast China. Cheng et al. (2014) showed that global warming may affect the climate in Gansu Province by shifting summer weather from a warm-dry to a warm-wet climate. This transition would result in increased precipitation in Gansu Province. However, the glaciers in the Qilian mountain range, the source of the Heihe River, have been steadily decreasing in mass since the 1970s (Xiao et al., 2007). With decreasing flow volume in the river, agricultural areas have migrated upstream, where water resources are more readily available (Li et al., 2013). As Hao et al. (2016) show, over a 50-year period, temperatures in the Tarim Basin have been consistently rising at a higher rate compared to other areas of China, as the result of two factors. First, temperatures across the basin are in fact rising. Secondly, the oasis effect is diminishing over time, resulting in a higher rate of temperature increase within the oasis. The authors conclude that the diminishing oasis effect is due to decreasing wind speed over northwest China, expansion of arid land and new water-saving agricultural techniques. Fang (2019) confirms this trend, observing that in recent years (2015–2018) the magnitude of the oasis effect has been diminishing in the Heihe river basin. These studies suggest that water availability will diminish and temperature will increase rapidly in northwest China's oases in the future, which, along with increasingly intense heatwaves, could pose risks to human health (Kang and Eltahir, 2018).

As Li et al. (2016) describe, knowledge gaps remain in modelling seasonal and diurnal oasis effects, as well as differences between air and surface temperature oasis effects. Most studies of the oasis effect either rely on field observation or numerical models, both of which have their benefits and challenges (Hao and Li, 2016). Previous observational studies have been limited in their scope and have not fully investigated the implications of surface versus air temperature oasis effects. Both Kai et al. (1997) and Potchter et al. (2008) used small data sets, collected over the course of several consecutive days during the summer, resulting in limited study scopes. Numerical models provide useful mechanistic explanations but often lack detail, and Li et al. (2016) recommend further study on small-scale impacts of land use change. Lobell et al. (2006) suggest that climate models would benefit from greater certainty of how irrigation affects regional climate. This study expands on previous research by investigating seasonal and diurnal oasis effects and provides detailed insight on energy balance dynamics resulting from land use change.

Using the theory of intrinsic biophysical mechanism (IBPM), this study provides a quantitative attribution of the oasis effect to individual biophysical factors. Developed by Lee et al. (2011), the IBPM theory was first used to describe local climatological effects of deforestation. It was then applied to surface temperature changes due to urbanization by Zhao et al. (2014), and later modified by Wang et al. (2018) in their investigation of afforestation surface temperature impacts. In this study, the IBPM theory is applied for the first time to the desert-oasis system, both to evaluate the theory's potential to accurately predict observed oasis effects and to provide a mechanistic explanation for the observed phenomenon. The oasis effect can be thought of an inverse urban heat island: land use change creates a temperature depression in artificial oases, whereas urbanization typically increases temperature.

The aims of the current study are to:

1. Characterize seasonal and diurnal trends of oasis effects, as well as differences between air and surface oasis effects, in Zhangye during the calendar year 2013
2. Evaluate the IBPM theory for predicting surface oasis effects
3. Provide insights on the surface energy balance mechanisms underlying the oasis effect
4. Suggest possible meteorological variables that significantly impact the magnitude of observed oasis effects

2. Materials and methods

2.1. Sites

The current population of Zhangye city is over 1.2 million, with an additional 770,000 people residing in the Heihe River Basin. Farmland surrounding Zhangye is irrigated by the Heihe River, the second longest inland river in China, which is fed by snowmelt from the Qilian Mountains to the west. The Heihe River Basin spans from 97.1° E to

102.0° E and 37.7° N to 42.7° N, with an approximate area of 143,000 km^2. Elevations in the agricultural mid-stream basin range from approximately 1000 to 3000 m (Liu et al., 2018). Water is a vital yet scarce resource in Zhangye: agriculture consumes 81% of the volume of the Heihe River, as 50% of farmland in Zhangye is fed by irrigation (Xu et al., 2014). Recent population growth has increased strain on water resources, resulting in a terminal lake of the Heihe River to the northeast of Zhangye having dried in the 1990s (Wang et al., 2015). With water being a scarce resource in the river basin, environmental managers in Zhangye must reach a compromise between diverting water for irrigation and reserving some for downstream ecosystem rehabilitation and other needs.

Precipitation and relative humidity in Zhangye and its surrounding agricultural areas remain low throughout the year. The majority of precipitation falls in the summer months (June, July and August), reaching a maximum average of 30 mm in August, due to the influence of summer monsoons (Sun et al., 2007). Winter months (December, January and February) are extremely dry, with precipitation values ranging from 1 to 3 mm per month. The annual total precipitation is 129 mm. Monthly relative humidity varies from 40% to 60%, with drier conditions in March, April and May. Temperatures peak in July and reach the lowest values in December and January, with an annual mean air temperature value of 6 °C (Kai et al., 1997).

The Heihe Watershed Allied Telemetry Experimental Research (HiWATER) project was launched in May 2012 in the Heihe River Basin to study the hydrology of arid ecosystems (Li et al., 2013; Liu et al., 2018). The data used in this study were taken primarily in 2013 from two HiWATER monitoring stations: Daman Oasis Super Station (located at 100.372° E, 38.856° N, with an elevation of 1556 m) and Huazhaizi Desert Steppe Station (located at 100.319° E, 38.765° N, with an elevation 1731 m; HiWATER, 2013). The stations were 11 km apart, with the oasis station located approximately 10 km southwest of the center of Zhangye city and the desert station located 11 km to the southwest of the oasis station and approximately 21 km southwest of the center of Zhangye. Fig. 1 is a LANDSAT satellite image of the study area, including Zhangye and its surrounding agricultural fields, with the two sites marked. Fig. 1 also shows recent land use change on a regional scale. The desert station was located in a desert steppe ecosystem with sparse vegetation (Fig. 2a). The oasis station was located in a corn field, where vegetation reached approximately 3 m during summer months (Fig. 2b). The crop was watered in the summer months via flood irrigation, during which water from the Heihe River was directed to the field via irrigation canals and flooded the field.

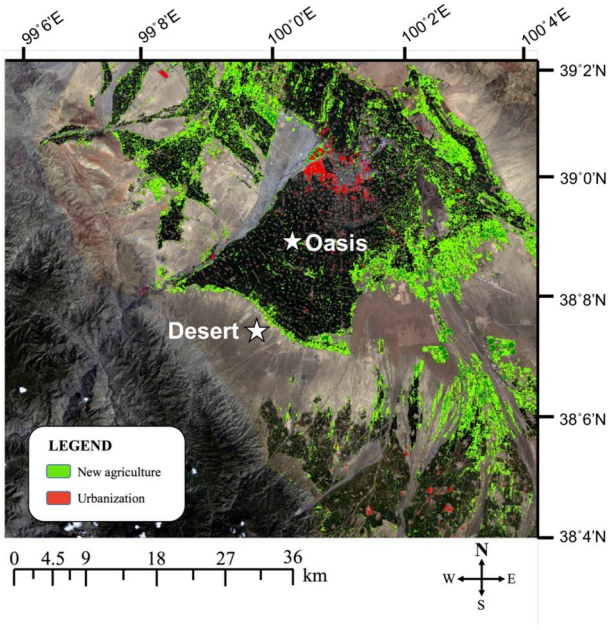

Fig. 1. The site of the oasis and desert stations, as well as land use change from 1991 to 2013. Locations of field sites are marked with white stars. Bright red areas represent urbanization, with a decrease in NDVI between 1991 and 2013 (negative change in NDVI ranging from −0.22 to −1.58). Bright and dark green areas represent new agricultural fields, with an increase in NDVI between 1991 and 2013 (positive change in NDVI ranging from +0.45 to +1.8). (For interpretation of the references to colour in this figure legend, the reader is referred to the Web version of this article.)

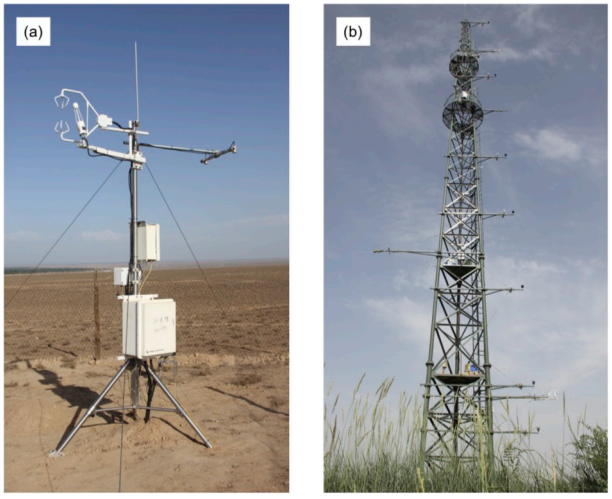

Fig. 2. (a) Huazhaizi Desert Steppe station and (b) Daman Oasis Superstation ground photographs.

2.2. Data

The HiWATER stations were equipped with eddy covariance systems, large aperture scintillometers, automatic weather stations, cosmic-ray neutron probes and wireless sensor networks. The datasets from the oasis and desert stations included the following variables at half-hourly intervals for the calendar year 2013: soil heat flux, latent and sensible heat fluxes, relative humidity, wind speed at several heights (0.5, 2.0, 2.0 and 3.0 m at the desert station and 3.0, 5.0, 10.0, 15.0, 20.0, 30.0 and 40.0 m at the oasis station), air temperature (1.0, 2.0 and 3.0 m at the desert station and 3.0, 5.0, 10.0, 15.0, 20.0, 30.0, and 40.0 m at the oasis station), precipitation, radiation (incoming and outgoing long-wave and short-wave), soil moisture, surface temperature and pressure (Li et al., 2013). Unphysical values are marked and rejected (Liu et al., 2011). Data were stratified into seasons by solar equinoxes and solstices. The data were averaged over summer, fall, winter and spring to distinguish diurnal trends, and time was converted to local solar time (+7 UTC).

Surface temperatures at both desert and oasis sites were calculated from outgoing longwave radiation ($L_{\uparrow}$) and the incoming longwave radiation ($L_{\downarrow}$) (Zhao et al., 2016):

$$T_s = \left(\frac{L_{\uparrow} - (1-\varepsilon)L_{\downarrow}}{\sigma\varepsilon}\right)^{\frac{1}{4}} \quad (2)$$

where ε is surface emissivity, assumed to be 0.98, and σ is the Stephan-Boltzmann constant.

To study the impacts of land use change, in this case from semiarid steppe to artificial oasis, this study defines the oasis effect (ΔT) as the difference in temperature between the oasis (T_o) and the adjacent dryland land (T_d):

$$\Delta T = T_o - T_d \quad (1)$$

The oasis is typically colder than the surrounding natural land, resulting in a negative ΔT. In this study, oasis effects are calculated using

both the land surface temperature (ΔT_s) and the near-surface air temperature (ΔT_a).

The surface temperature oasis effect (ΔT_s) was calculated as the difference between oasis and desert surface temperatures. Because each station was equipped with air temperature measurements at several heights, air temperature oasis effects (ΔT_a) were calculated as the difference in temperature between the oasis and desert stations at various heights to account for vegetation growth in the oasis in summer, when crops reach a peak of 3 m in height. In the afternoon, ΔT_a was shown to be most negative between the oasis 3-m air temperature reading and the desert 1-m air temperature reading throughout the year, and therefore measurements at these heights will be used as the default in this study. In the online supplement, we also present the ΔT_a calculations using different combinations of measurement heights between the two stations (Supplementary Fig. 1).

A small lapse rate correction was applied to the oasis effects to account for the elevational difference between the two sites. Assuming a standard lapse rate of 0.0065 K m^{-1}, we expect that the cropland site to be 1.1 K warmer in the absence of the oasis effect. In the following, the oasis effect (both surface temperature and air temperature) is the computed temperature difference minus this background temperature offset of 1.1 K.

2.3. Application of the IBPM theory

Using a one-source representation of the surface-air exchange of heat, the theory expresses the surface temperature (K) as (Lee et al., 2011),

$$T_s = \frac{\lambda_0}{1+f}(R_n^* - G) + T_a \tag{3}$$

where T_a is air temperature (K) above the surface, f is a dimensionless energy redistribution factor, λ_0 is the local climate sensitivity, which is a weak function of temperature, G is ground heat flux (W m^{-2}), and R_n^* is apparent net radiation (W m^{-2}) given by

$$R_n^* = S + L_\downarrow - \sigma T_a^4 \tag{4}$$

where S is net shortwave radiation (W m^{-2}), and $L_\downarrow$ is incoming longwave radiation (W m^{-2}). The energy redistribution factor f (dimensionless) is defined as

$$f = \frac{\rho c_p}{4 r_T \sigma T_a^3}\left(1 + \frac{1}{\beta}\right) \tag{5}$$

where ρ is air density, c_p is the specific heat of air, β is Bowen ratio and r_T is the total heat transfer resistance.

Equation (1) can be differentiated to obtain the following equation:

$$\Delta T_s = \frac{\lambda_0}{1+f}(\Delta S + \Delta L_\downarrow) + \frac{-\lambda_0}{(1+f)^2}(\Delta R_n^* - G)\Delta f + \frac{-\lambda_0}{1+f}\Delta G + \left(\Delta T_a - \frac{\lambda_0}{1+f}\sigma \Delta T_a^4\right) \tag{6}$$

where Δ denotes the difference between oasis and desert sites (oasis value minus desert value). Here, the surface temperature perturbation ΔT_s (or the surface oasis effect) can be interpreted as the consequence of a local longwave radiation feedback and energy redistribution between the surface and the overlaying atmosphere. The first term on the right-hand side of the equation represents the effect of differences in radiative forcing (albedo) between the two sites, the second term represents Bowen ratio differences between the two sites, the third term represents ground heat flux differences between the two sites, and the final term represents air temperature differences between the two sites. Incoming shortwave radiation was assumed to be equal between the two sites to minimize instrument error, and this assumption improved the performance of the theory. With this assumption, ΔS results from the albedo difference between the oasis and the desert sites.

Three modifications are made to the original formulation presented by Lee et al. (2011). First, in the original formulation, f is computed from a parameterization of the aerodynamic heat resistance r_T, and in doing so energy imbalance inherit in eddy covariance measurements can cause large errors in the application of Equation (6) (Wang et al., 2018). Here we determined the f value by inverting Equation (3) using ΔT_s, ΔT_a, R_n^*, and G produced by MERRA-2 reanalysis (Chakraborty and Lee, 2019) for the reanalysis gridcell centered at Zhangye. The period used was 2008–2017, and the annual daytime and nighttime mean f values are 5.01 and 1.79, respectively. A similar method was deployed by Bright et al. (2017) to compute the energy redistribution factor for the major biome types across the world. Our mean f (3.39, the mean of daytime and nighttime values) is similar to that reported by Bright et al. (2017) for irrigated croplands (3.29, with a 1.4 root mean square deviation), and our nighttime value is similar to that reported by Cao et al. (2016) for Northwest China (1.3 ± 1.8).

Second, the change in f due to changes in the Bowen ratio is given by:

$$\Delta f = \frac{\rho_d c_p \lambda_0}{r_T}\left(\frac{\Delta\beta}{\beta^2}\right) \tag{7}$$

where $\Delta\beta$ is the difference in the Bowen ratio between the two sites. Eliminating r_T in favor of f from Equations (5) and (7), we obtain

$$\Delta f = \frac{\Delta\beta f}{\beta^2\left(1 + \frac{1}{\beta}\right)} \tag{8}$$

Thus Equation (8) allows us to quantify the contribution of the Bowen ratio changes to ΔT_s without the need to parameterize the heat resistance.

Third, changes in f can also be caused by changes in r_T between the two sites. However, calculation of r_T can be avoided by substituting Equation (8) into Equation (7). Thus r_T is omitted in the present study. The good agreement between the observed ΔT_s and the ΔT_s estimated from Equation (6) confirms that this omission is reasonable.

Seasonal albedo was calculated as the average ratio of incoming shortwave to outgoing shortwave incoming radiation. The local intrinsic climate sensitivity λ_0 was calculated as

$$\lambda_0 = \frac{1}{4\sigma T_a^3} \tag{9}$$

All other terms were obtained directly from the HiWATER dataset.

2.4. Correlation analysis

The IBPM theory is valid for only the surface temperature perturbation. To also understand drivers of the air temperature oasis effect, we performed analyses of its correlation with various meteorological variables. Correlation analyses were also performed on the surface temperature oasis effect. The key predictors in these correlation analyses are atmospheric clarity, wind speed and wind direction.

For the wind direction correlation analysis, data were stratified into two groups by wind direction at the desert site: northeast wind (from the oasis) or southwest wind. Wind blowing from the cool oasis into the warm desert was hypothesized to result in a smaller oasis effect, as desert temperatures would be depressed. A t-test was run to determine whether the observed oasis effects at 13:30, when the magnitude of the summer surface temperature oasis effect was greatest, were significantly different as a result of wind direction. Linear regression was used to determine the relationship between desert windspeed (measured at 1 m) and oasis effect data.

Data were also stratified by a clarity index to determine the impact of atmospheric clarity on the oasis effect in each season. Oasis effect data were stratified into cloudy and clear days. Following Gu et al. (1999), the clearness index (k_t) is defined as

$$k_t = \frac{S}{S_e} \tag{10}$$

where S is observed solar radiation at the surface and S_e is extra-terrestrial radiation at top of atmosphere. Data were stratified based on

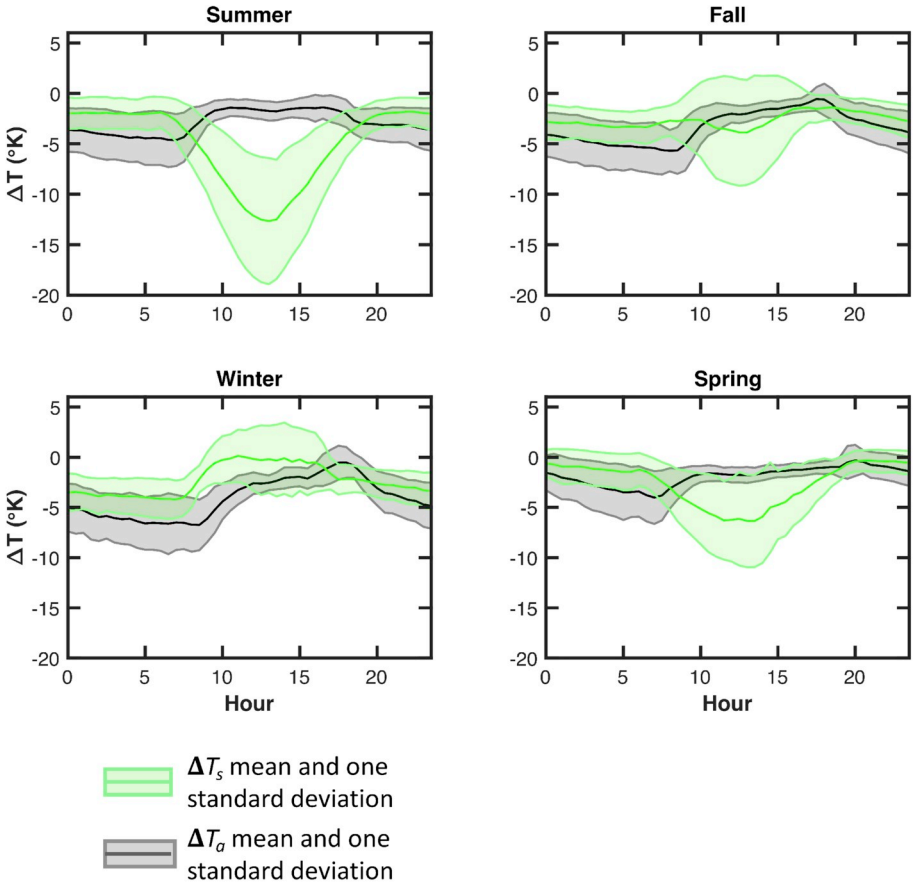

Fig. 3. Diurnal composites of air temperature and surface temperature oasis effects in four seasons of 2013. Dark green lines represent average surface temperature oasis effects (the difference in surface temperature between oasis and desert sites), with shaded green areas representing one standard deviation. Dark back lines represent average air temperature oasis effects (the difference in air temperature between oasis and desert sites), with shaded gray areas representing one standard deviation. Time is local solar time (+7 UTC or Beijing time minus 1 h). (For interpretation of the references to colour in this figure legend, the reader is referred to the Web version of this article.)

values of k_t where values 0 « 0.5 were marked as cloudy days and values $0.65 < k_t < 1.0$ were marked as sunny days. Days with values $0.5 < k_t < 0.65$ were discarded in the analysis.

Multivariable correlation analysis was performed to quantify the relationship between wind speed, clarity index, and oasis effects. Data obtained at 13:30 (local solar time) for each season were fitted with multivariate regression models, with clarity index and wind speed as predicting variables.

3. Results and discussion

3.1. General features of the oasis effect

Fig. 3 shows results of the statistical analyses of diurnal trends in ΔT_a and ΔT_s in each season. Clear diurnal and seasonal trends are observed for both ΔT_a and ΔT_s, which follow surprisingly divergent patterns. While ΔT_s reaches the most negative values during daylight hours in summer, fall and spring, with values of −12.7, −3.9 and −6.4 K, respectively, ΔT_a reaches its most negative values during nighttime, with values of −4.6, −5.7, −6.8 and −4.1 K in summer, fall, winter and spring respectively. The surface oasis ΔT_s is observed most strongly in the summer afternoon at 13:30 (local solar time), when ΔT_s reaches an average of −12.7 ± 6.6 K. A large negative ΔT_s is also observed in the afternoon in spring. In fall, ΔT_s is less pronounced in the afternoon, and in winter, the trend is reversed, with a more dramatic winter ΔT_s in the early morning than in the afternoon (reaching its most negative value of − 4.2 K at 7:00). In summer, ΔT_a (−1.7 ± 1.0 K) is significantly smaller than ΔT_s at 13:30. In each season, the ΔT_a is more negative at night than ΔT_s and experiences less variability throughout the day, with ΔT_s having a larger standard deviation during daylight hours. Further analysis concentrates primarily on summer at 13:30 as ΔT_s is most pronounced in summer afternoon.

Fang (2019) showed that daytime surface temperature oasis effect values (warm season average from May to September) in Zhangye ranged between −10 and −20 K over the period from 2001 to 2015. Cold/dry season average oasis effect values (September to May) ranged from −6 to −8 K. Our results are within these ranges, suggesting that 2013 is a typical year at the field site.

With ΔT_s being greater during the afternoon in summer, fall and spring, results contrast with findings by Potchter et al. (2008), who observed more intense surface temperature oasis effects at night than in the day during summer months. The strong ΔT_s observed in the afternoon during spring, fall and summer and its greater standard deviation than at night suggest that insolation may have a significant impact on the oasis effect, as more energy enters the system during these hours.

Our results suggest an even greater maximum ΔT_s than the −7 K effect observed by Kai et al. (1997) between air temperature readings at the height of 1 m above the ground. Furthermore, Hao and Li (2016) reported average daytime oasis effects of −9.08, −4.24 and −3.85 K for an oasis in the Tarim Basin for summer, fall and spring, respectively. Similar to our conclusions, Hao and Li (2016) also found ΔT_s is smaller at night than during the day, and the most intense ΔT_s occurs during the summer. Our findings suggest that the oasis effect in Zhangye is more pronounced than in other arid regions, perhaps implying higher irrigation intensity in Zhangye than the studies cited above. Another possible explanation is landscape contracts that enable greater rates of heat advection and therefore enhance latent heat flux and minimize sensible heat flux over the oasis site.

Air temperature data from various heights were averaged for the summer, shown in Fig. 4. At 3 m, the oasis experiences a greater diurnal temperature range (12.41 K) than the desert site at 1 m (9.43 K) does. Both stations experience an inversion during the nighttime. At the oasis site, a thermal inversion starts at 17:00 and lasts until 8:00. At the desert site, the inversion period lasts on average between 18:30 and

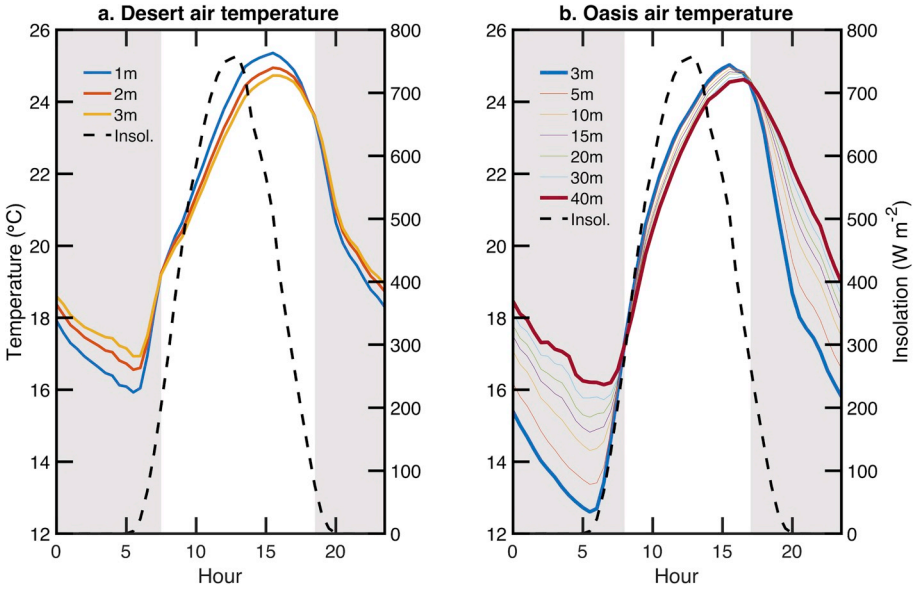

Fig. 4. Diurnal composites of air temperatures at several heights above (a) desert and (b) oasis stations in the summer of 2013 with mean incoming shortwave radiation marked in dashed black lines. Gray shading denotes thermal inversion period.

7:30. A nighttime inversion was also observed in fall, winter, and spring at both sites. At 13:30, when ΔT_s is most pronounced, the oasis station showed a smaller temperature gradient across 37 vertical meters than the desert station does across 2 vertical meters, implying intense vertical mixing at the oasis site and less mixing at the desert site. This would increase the horizontal temperature gradient between oasis and desert sites, with intensive latent heat flux at the oasis site leading to a cooling effect. This result confirms the theory that intense convection occurs over irrigated cropland, despite strong evaporative cooling, throughout the day.

A common perception, supported by short field campaigns such as that described by Kai et al. (1997), is that evaporative cooling near the surface should produce an inversion during the day. Fig. 4b shows that an inversion was present only in the later afternoon. This result should not be interpreted as a contradiction to the conclusion of Kai et al. (1997) because our result was based on seasonal mean temperatures, whereas theirs was restricted to five fair weather days. It is possible that an irrigation event immediately preceded their observational period. Suyker and Verma (2008) found that the midday surface Bowen ratio was negative for about one third of the growing season days of an irrigated corn-soybean ecosystem in Nebraska, USA, where the mean growing season precipitation (450 mm from May to September) is similar to that in Zhangye (130 mm). In their study, the switching of Bowen ratio from being positive to being negative, the latter of which implies inversion conditions, coincided with irrigation events. The daytime variation in the static stability at the oasis site (Fig. 4b) is consistent with the diurnal composite sensible heat flux in the summer showing positive values before and negative values after 17:00 (Supplementary Fig. 2). In agreement with our study, Li et al. (2016) observed a change in static stability from being unstable to being stable (or inversion) in mid-afternoon. The five-day mean sensible heat flux curve given by Kai et al. (1997) suggests that such switching had also occurred during their experiment (although at an earlier time of 12:00 than ours).

3.2. Attribution of the surface oasis effect

The IBPM theory was applied to provide a mechanistic understanding of the observed trends in ΔT_s discussed above. Table 1 shows intermediate values by season at 13:30 before multiplication by the IBPM coefficients. Unsurprisingly, the oasis site has higher evaporation rate (Supplementary Table 1) and a lower Bowen ratio than the desert site in all the seasons. This negative Bowen ratio difference should lead to a negative ΔT_s. In contrast, the oasis site absorbs ground heat flux difference ΔG is positive in summer and fall and negative in winter and spring. This result suggests that ground heat flux at the desert site is larger in magnitude during winter and spring than at the oasis site, and ground heat flux is larger in magnitude at the oasis site during summer and fall. Therefore, the ground heat flux should decrease the oasis effect (making ΔT_s more positive) during winter and spring months but increase it (making ΔT_s more negative) during fall and summer. In other words, ground heat flux should partially offset evaporative cooling effects in spring and winter, while exaggerating evaporative cooling effects in summer and fall.

Table 1
Seasonal mean intermediate variables at 13:30 used in the IBPM calculation (oasis value minus desert value).

Season	ΔS (W m^{-2}) Radiative forcing	Δβ (dimensionless) Bowen ratio changes	ΔG (W m^{-2}) Soil heat flux	ΔT_a (K) Air temperature changes
Summer	49.4	−1.06	42.1	−0.65
Fall	59.4	−3.19	48.4	−0.91
Winter	67.4	−0.25	−17.7	−1.45
Spring	20.1	−3.21	−13.1	−0.68

Results of the IBPM calculations are presented in Figs. 5–7 for daytime hours (9:00 to 19:00). Nighttime (19:00 to 9:00) IBPM values are not presented in this study, as latent and sensible heat fluxes at night were near-zero (see Supplementary Fig. 2) or marked as unphysical, thus resulting in erratic nighttime Bowen ratios. Future studies should address nighttime Bowen ratio values in order to model the oasis effect at all times of day.

Fig. 5 compares the results of the IBPM theory for daylight hours in each season versus observed daytime variations in ΔT_s. A *t*-test was used to calculate whether a statistically significant difference existed between model results and observations, with a Bonnferroni correction used to set the p-value equal to 0.00238. The theoretical calculation (Equation (6)) is most accurate in summer and fall. In summer, calculated ΔT_s at 13:30 (−12.9 ± 1.8 K) closely approximates observed ΔT_s (−12.6 ± 6.6 K) for peak oasis effects at 13:30, with an RSME value of 3.11 K ($p = 0.057$). The model most closely predicts summer ΔT_s at

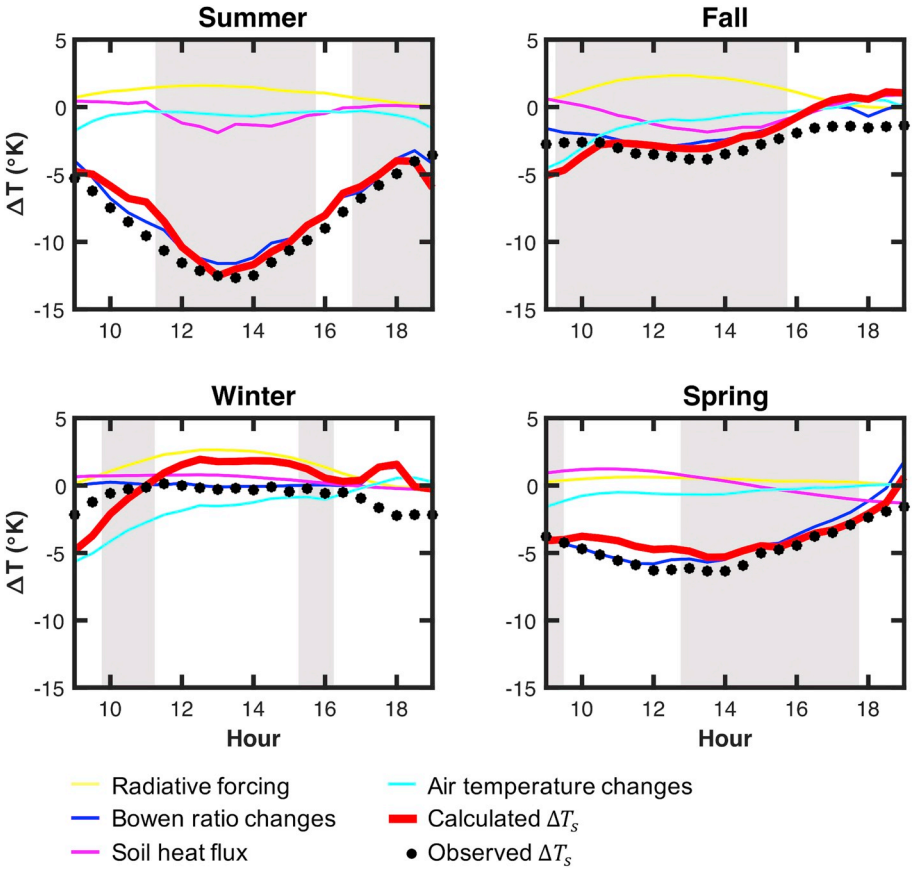

Fig. 5. IBPM results for 2013 by season from 9:00 to 19:00 (daylight hours). Red lines, calculated surface temperature oasis effects; Black dots, observed surface temperature oasis effects; Yellow lines, contribution from radiative forcing; Dark blue lines, contribution from Bowen ratio change; Pink lines, contribution from soil heat flux forcing; Light blue lines, contribution from air temperature difference. Gray shading denotes times at which there is no statistical difference between model results and observations ($p > 0.00238$). (For interpretation of the references to colour in this figure legend, the reader is referred to the Web version of this article.)

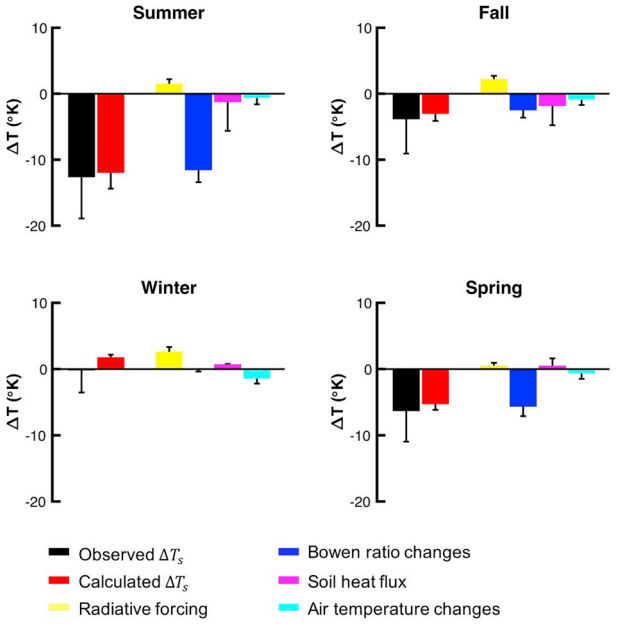

Fig. 6. IBPM theory results at 13:30 by season. Black bars: observed surface temperature oasis effect; Red bars: calculated average surface temperature oasis effect; Yellow bars: contribution from radiative forcing; Dark blue bars: contribution from Bowen ratio change forcing; Pink bars, contribution from soil heat flux change; Light blue bars, contribution from air temperature change. Error bars are ± 1 standard deviation. (For interpretation of the references to colour in this figure legend, the reader is referred to the Web version of this article.)

14:30 and 18:00 ($p = 0.56$ and 0.98 with RSME values of 4.55 and 4.23 K, respectively), and successfully predicts observational data for 66% of the half-hourly daytime intervals. For fall, the IBPM model is most successful in mid-morning and mid-afternoon, with no statistical difference between model and observation between 9:30 and 15:30, predicting 61% of the daytime half-hourly intervals. For summer and fall, the hours for which the IBPM is most successful correspond with the hours of intense insolation, which intensifies latent heat flux. In spring, the IBPM model successfully predicts 57% of the daytime half-hourly intervals, the majority of which are in the late afternoon (13:00 to 18:00). The IBPM model is less successful in winter, with only 23% of model results correctly predicting observed ΔT_s. This may be an effect of the sun's rising later in the day, and therefore less convection at the two sites in early morning, and the minimal effect of the Bowen ratio change. These findings suggest IBPM theory most accurately models ΔT_s during daylight hours, when air temperature differences are less pronounced and evaporative cooling enhances Bowen ratio differences, and that the coefficient for air temperature differences should be modified to address diurnal variations in convection. As discussed below, latent heat flux is a main driver of ΔT_s, and evaporation caused by insolation is closely related to the success of the model. In summary, the IBPM theory can closely approximate the sign and magnitude of average surface temperature oasis effects from 11:30 to 15:30 and 17:00 to 19:00 in summer, 9:30 to 15:30 in fall, 10:00 to 11:00 and 15:30 to 16:00 in winter, and 13:00 to 18:00 in spring.

Fig. 6 shows average individual contributions to the total oasis effect at 13:30 for each season with standard error. For each season, the IBPM theory closely approximates the magnitude of ΔT_s at 13:30. In summer, a positive ΔS contribution is outweighed by negative $\Delta\beta$, ΔG and ΔT_a contributions, resulting in a predicted ΔT_s of −12.9 K, which is very close to the observed value of −12.0 K. Similarly, in fall a positive

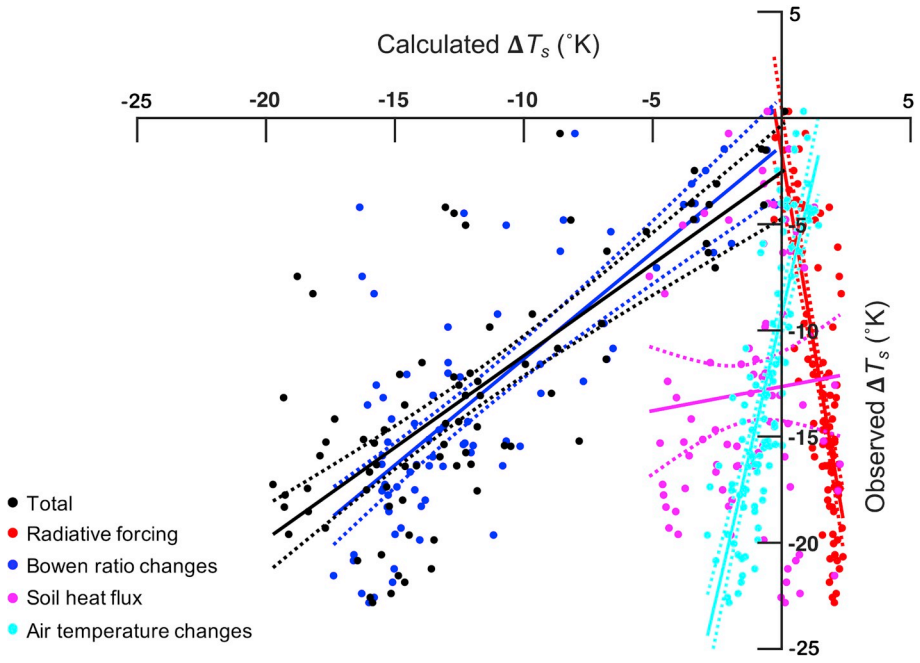

Fig. 7. Comparison of IBPM calculations with the observed oasis effect at 13:30 on individual days throughout summer 2013. Red dots: contribution from radiative forcing; Blue dots, contribution from Bowen ratio changes; Pink dots: contribution from soil heat flux change; Light blue dots: contribution from air temperature changes; Black dots: sum of component contributions. Sold lines represent linear regression for each component, with surrounding dotted lines representing one standard error. (For interpretation of the references to colour in this figure legend, the reader is referred to the Web version of this article.)

ΔS contribution is balanced by negative $\Delta\beta$, ΔG and ΔT_a contributions, with a predicted ΔT_s of −3.1 K within one standard error of the observed ΔT_s(− 3.9 K). In winter, the larger positive ΔS and small positive ΔG outweigh the negligible $\Delta\beta$ and small negative ΔT_a, resulting in a small positive predicted ΔT_s of 1.8 K, which is slightly greater than the observed ΔT_s of − 0.20 K. In spring, a large negative $\Delta\beta$ and small negative ΔT_a, with small positive ΔS and ΔG forcings, result in a negative ΔT_s of −5.3 K, similar to the observed value of − 6.4K. Differences between the model and observational data are statistically insignificant for summer, fall, and spring at 13:30, with p-values of 0.057, 0.196, and 0.013, respectively. In summer especially, Bowen ratio changes dominate the oasis effect, resulting in a large negative ΔT_s. The diminished $\Delta\beta$ in winter is due to the lack of irrigation in winter months, resulting in dry conditions and limited latent heat flux over the oasis.

Fig. 7 plots component contributions (horizontal axis) against the observed surface oasis effect (vertical axis). Linear regression lines are shown in Fig. 7, and the regression statistics are given in Table 2. In this plot, each data point represents a half-hour observation for 13:30 in the summer (a total of 92 days). The Bowen ratio contribution most closely approximates the observed surface temperature oasis effect, both in slope and intercept, indicating that ΔT_s is most sensitive to the difference in Bowen ratio between the cropland and the desert site. The ground heat flux plays a minor role in determining the oasis effect. The contribution from albedo changes has a small negative slope with respect to the observed oasis effect, indicating once again that the role of the albedo is to reduce the oasis strength, as the oasis absorbs more energy from insolation than the desert. This result further confirms that latent heat flux is the main predictor of the magnitude of the surface temperature oasis effect in summer.

Table 2
Linear regression details for Fig. 7.

Forcing	R^2	Slope	Intercept
Total	0.57	0.86	−1.45
Radiative forcing	0.59	−7.22	−0.58
Bowen ratio changes	0.60	1.00	−0.21
Soil heat flux	0.005	0.23	−11.54
Air temperature changes	0.66	5.26	−8.16

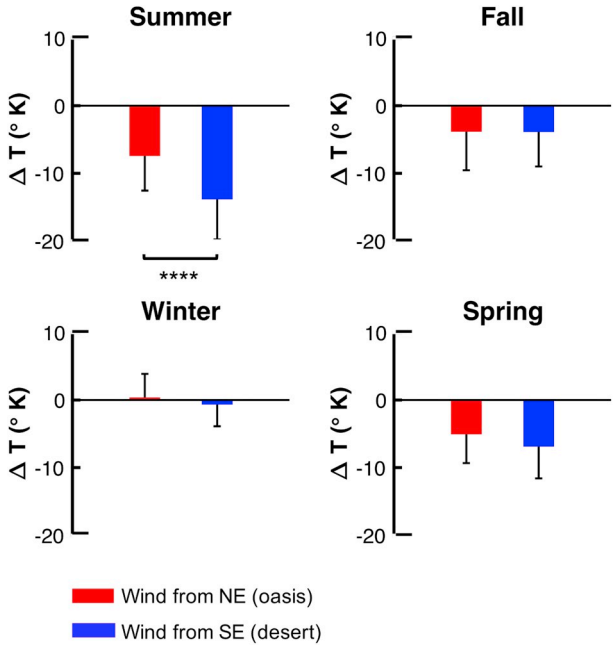

Fig. 8. Comparison of the surface temperature oasis effect at 13:30 between two wind direction sectors. Blue bars: southeast wind. Red bars: northeast wind. Error bars are ± one standard deviation. Significance is denoted by stars. (For interpretation of the references to colour in this figure legend, the reader is referred to the Web version of this article.)

3.3. Correlation analysis

Figs. 8 and 9 show the results of the wind direction analysis. Wind direction had a statistically significant effect on the ΔT_s and ΔT_a in summertime at 13:30, with greater oasis effects observed when wind blew from the southwest (from the desert towards the oasis) than from the northwest (from the oasis to the desert). This result confirms our hypothesis that wind blowing from the cool oasis into the warm desert depresses desert temperatures and minimizes the oasis effect. Desert surface and air temperatures were found to be significantly lower when wind blows from the northeast, with stratified desert surface

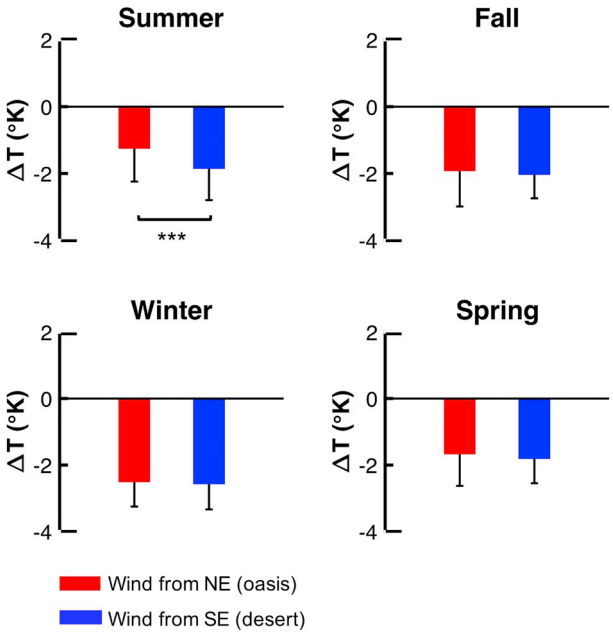

Fig. 9. Comparison of the air temperature oasis effect at 13:30 between two wind direction sectors. Blue bars: southeast wind. Red bars: northeast wind. Error bars are ± one standard deviation. Significance is denoted by stars. (For interpretation of the references to colour in this figure legend, the reader is referred to the Web version of this article.)

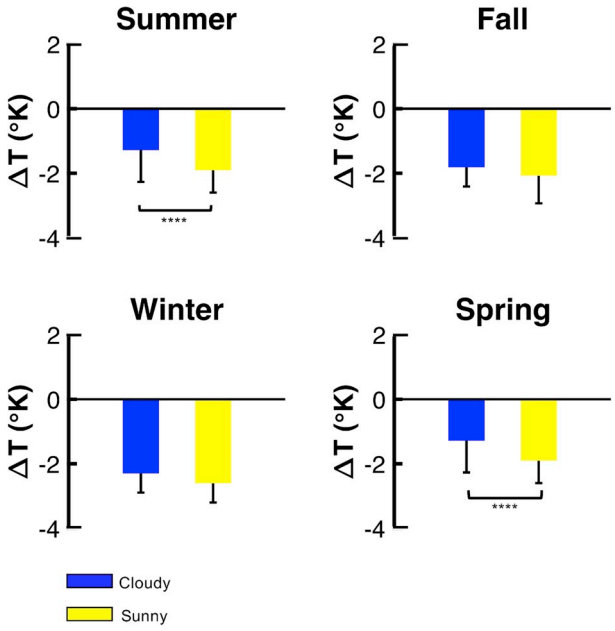

Fig. 11. Comparison of the surface temperature oasis effect at 13:30 between two sky conditions. Blue bars: cloudy conditions (with $0 < k_t < 0.5$); Yellow bars: sunny conditions (with $0.65 < k_t < 1.0$). Error bars are ± one standard deviation. Significance is denoted by stars. (For interpretation of the references to colour in this figure legend, the reader is referred to the Web version of this article.)

temperature data sets differing by 11.1 K on average (39.3 and 28.2 K mean surface temperature for SW and NE wind, respectively). Summertime oasis temperatures were also depressed with NE wind, although less dramatically than desert surface temperatures. For spring, fall and winter, wind direction did not have a significant impact on oasis effects.

Linear regression was used to investigate the impact of wind speed on the air temperature and surface temperature oasis effect. Fig. 10 shows the results of these analyses, with R^2 and p-values shown for significant linear relationships. In summer, fall and winter, wind speed had a significant impact on ΔT_s, with stronger wind resulting in more negative ΔT_s. Wind speed had a significant positive relationship to latent heat flux at the oasis site, implying increased evaporative cooling with higher wind velocity. In spring and summer, wind speed also had significant impacts on ΔT_a, with stronger wind resulting in more negative oasis effects. This result contrasts with the conclusions of Taha et al. (1991) and Potchter et al. (2008) that high wind velocity decreases the oasis effect. This difference may result from local topography and the short time scales of the two studies, which took place

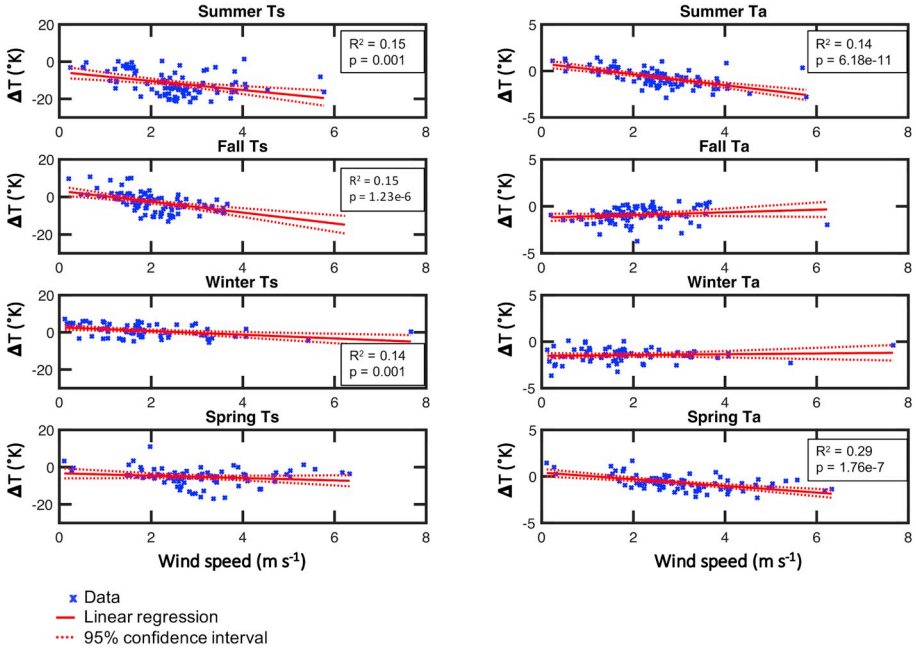

Fig. 10. Linear correlation of 13:30 surface and air temperature oasis effects with wind speed. Significant p-values and R^2 values are noted in black boxes (when p-values are significant).

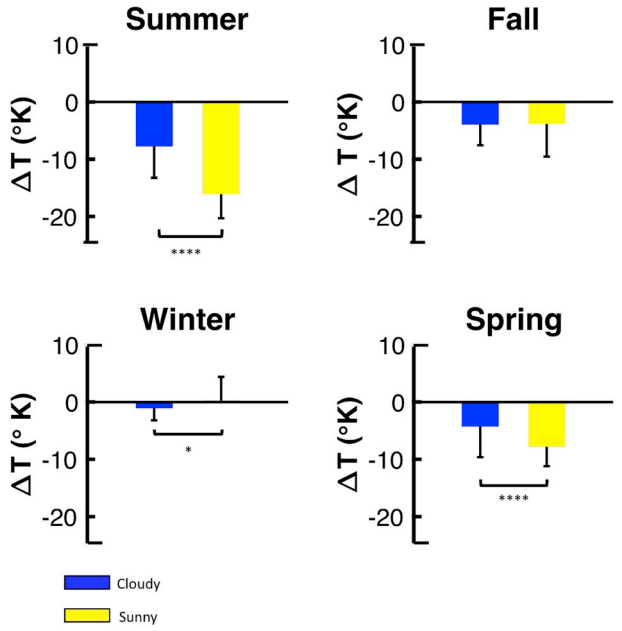

Fig. 12. Comparison of the air temperature oasis effect at 13:30 between two sky conditions. Blue bars: cloudy conditions (with $0 < k_t < 0.5$); Yellow bars: sunny conditions (with $0.65 < k_t < 1.0$). Error bars are ± one standard deviation. Significance is denoted by stars. (For interpretation of the references to colour in this figure legend, the reader is referred to the Web version of this article.)

over the course over several days. However, it confirms Hao et al. (2016)'s findings that diminishing wind speed over northeast China has resulted in weaker oasis effects.

Figs. 11 and 12 show the results of the atmospheric clarity analysis. Summer and spring ΔT_s and ΔT_a have significant differences between cloudy and clear days, with clear days resulting in significantly more negative oasis effects than cloudy days. This is perhaps due to increased evaporation with more energy entering the system, and therefore a larger Bowen ratio forcing. Hao et al. (2016) found a strong correlation between oasis cold island effects and incoming insolation, defining net incoming radiation as a key indicator of the intensity of the oasis effect. Significant differences between ΔT_s also appear in winter, but with sunny days producing a more positive ΔT_s. This result is likely due to a larger albedo forcing during winter months, when the desert site is de-vegetated, resulting in a more positive ΔS forcing. In fall, there was no significant impact of cloudy and clear days on ΔT_s or ΔT_a.

Table 3 shows the results of a two-variable correlation between oasis effects, wind speed, and clarity index for each season. In every season, stronger winds and clear conditions produce a significantly stronger surface temperature oasis effect. In summer, this relationship is strongest, with an R^2 value of 0.648, and is highly determined by clarity index with a coefficient of −19.24. Further analysis showed that stronger wind increased sensible heat flux at the desert site. This finding suggests that the magnitude of summertime ΔT_s is largely driven by the Bowen ratio partitioning. Under clear conditions, latent heat flux increases, producing a cooling effect in the oasis. In winter, clarity index has little impact on surface temperature oasis effect, with a small coefficient of −0.47, roughly 40 times smaller than in summer. During winter, dry conditions prevent intensive evaporation and limit the cooling effects of latent heat flux in the oasis. The positive offsets in each season, that is positive ΔT_s if k_t and U are both set to 0, seems to confirm that latent heat flux driven by insolation and sensible heat flux driven by wind result in a temperature depression within the oasis.

In each season, clarity and wind speed have weaker effects on ΔT_a than on ΔT_s. In summer and spring, clear conditions and higher windspeed produce a stronger ΔT_a with R^2 values of 0.535 and 0.515 respectively. In fall, this relationship is more scatted, with an R^2 value of 0.215, and windspeed has almost no effect on ΔT_a. In winter, the relationship between clarity, windspeed and ΔT_a is not significant.

4. Conclusions

With rising temperatures around the world and the ever-increasing threat of desertification, understanding the mechanisms of fragile oasis ecosystems is critical to sustainable management. This paper shows that latent heat flux is the driver behind a large cooling effect during daylight hours in summer, spring and fall in the Zhangye oasis. A novel contribution of this study to the oasis literature is a quantitative attribution of the oasis effect to individual biophysical factors through the IBPM theory. A largely successful mechanistic model of ΔT_s for daylight hours in a desert/oasis environment is produced by the IBPM theory, showing that the theory is applicable in contexts beyond which it was developed. Correlation analysis provides insights into the meteorological variables that influence the oasis effect. As Hao et al. (2016) found, diminishing oasis effects in northwest China are linked with diminishing wind speeds. Our results confirm that higher winds producer stronger ΔT_s in every season and diminishing winds result in significantly weaker surface temperature oasis effects.

This paper also shows that:

1. A significant surface temperature oasis effect is observed between the two field sites during afternoon hours in summer, spring and fall.
2. Air and surface temperature oasis effects follow opposite diurnal trends, with ΔT_a being more negative at night and ΔT_s more negative during daylight hours for summer, spring and fall. This difference is likely due to intense vertical convection at the oasis site during daylight hours.
3. IBPM theory successfully models average ΔT_s throughout the year during the majority of daylight hours for summer, fall, and spring, with Bowen ratio changes being most predictive of observed surface oasis effects in summer months.
4. Wind direction significantly impacts ΔT_s and ΔT_a during the summer, with wind from the NE depressing desert surface temperatures and therefore minimizing oasis effects.
5. Wind speed and atmospheric clarity have a significant impact on ΔT_s in every season, with clear conditions and high wind speeds

Table 3
Multi-variate correlation of wind speed, clarity and oasis effect.

Season	Oasis effect	Equation (U wind speed (m s^{-1}) and k_t clarity index)	R^2	RMSE	P-value
Summer	Surface	$\Delta T_s = -1.3\,U - 19.24\,k_t + 3.71$	0.648	3.77	6.59e-21
	Air	$\Delta T_a = -0.49\,U - 1.66\,k_t + 0.60$	0.535	0.667	1.57e-15
Fall	Surface	$\Delta T_s = -1.80\,U - 20.17\,k_t + 13.12$	0.496	3.76	1.15e-13
	Air	$\Delta T_a = -0.003\,U + 2.66\,k_t - 3.75$	0.215	0.72	2.64e-05
Winter	Surface	$\Delta T_s = -0.99\,U - 0.47\,k_t + 1.93$	0.148	3.15	0.0046
	Air	$\Delta T_a = 0.04\,U + 0.40\,k_t - 2.90$	0.013	0.747	0.649
Spring	Surface	$\Delta T_s = -0.47\,U - 11.50\,k_t + 2.58$	0.367	3.37	1.45e-8
	Air	$\Delta T_a = -0.33\,U - 1.61\,k_t + 0.29$	0.515	0.563	4e-13

increasing the magnitude of the effect. Atmospheric clarity has a significant impact on ΔT_s and ΔT_a in summer and spring by increasing ΔT_s on sunny days, while clear days result in more positive ΔT_s in winter.

This study is limited in that the data used are only from 2013 and from two sites. Therefore, future studies should incorporate data from other years and sites to determine whether the trends observed in this study are similar to other locations. Future research should also take into account surface roughness in calculating IBPM theory energy distribution. Finally, more in-depth analysis of meteorological conditions that impact the oasis effect is needed.

CRediT authorship contribution statement

Sophie Ruehr: Software, Formal analysis, Writing - original draft, Visualization. **Xuhui Lee:** Conceptualization, Methodology, Writing - original draft, Supervision. **Ronald Smith:** Validation, Supervision. **Xin Li:** Data curation, Resources, Supervision. **Ziwei Xu:** Data curation, Resources, Supervision. **Shaomin Liu:** Resources, Supervision. **Xiaofan Yang:** Resources, Supervision. **Yanzhao Zhou:** Resources, Investigation.

Declaration of competing interest

The authors declare that they have no known competing financial interests or personal relationships that could have appeared to influence the work reported in this paper.

Acknowledgements

We thank Bowen Fang, Natalie Schultz and TC Chakraborty for helpful comments. Funding for travel (to SR) to the field site was provided by the Yale University Department of Geology & Geophysics Karen Von Damm '84 Fellowship.

Appendix A Supplementary data

Supplementary data to this article can be found online at https://doi.org/10.1016/j.jaridenv.2020.104120.

References

Bright, R., Davin, E., O'Halloran, T., Pongratz, J., Zhao, K., Cescatti, A., 2017. Local temperature response to land cover and management change driven by non-radiative processes. Nat. Clim. Change 7, 296–304.
Cao, C., Lee, X., Liu, S., Schultz, N., Xiao, W., Zhang, Mi, Zhao, L., 2016. Urban heat islands in China enhanced by haze pollution. Nat. Commun. 7.
Chakraborty, T., Lee, X., 2019. Land cover regulates the spatial variability of temperature response to the direct radiative effect of aerosols. Geophys. Res. Lett. 46, 8995–9003.
Cheng, G., Li, X., Zhao, W., Xu, Z., Feng, Q., Xiao, S., Xiao, H., 2014. Integrated study of the water–ecosystem–economy in the Heihe River Basin. Natl. Sci. Rev. 1, 413–428.
Douglas, E., Beltran-Przekurat, A., Niyogi, D., Pielke Sr, R., Vörösmarty, C.J., 2009. The impact of agricultural intensification and irrigation on land–atmosphere interactions and Indian monsoon precipitation — a mesoscale modeling perspective. Glob. Plant. Chang. 67, 117–128.
Eziz, M., Yimit, H., Mohammad, A., Zhifang, H., 2010. Oasis land-use change and its effects on the oasis eco-environment in Keriya Oasis, China. Int. J. Sustain. Dev. World Ecol. 17, 244–252.
Fang, B., 2019. Characteristics of Oasis Effect in Zhangye, China and its Relationship with Agricultural Irrigation. Master's Project Report School of Forestry and Environmental Studies, Yale University available at: https://xleelab.sites.yale.edu/sites/default/files/files/fang_yale_2019.pdf.
Gu, L., Fuentes, J.D., Shugart, H.H., Staebler, R.M., Black, T.A., 1999. Responses of net ecosystem exchanges of carbon dioxide to changes in cloudiness: results from two North American deciduous forests. J. Geophys. Res. 104 (D24), 31421–31434.
Hao, X., Li, W., 2016. Oasis cold island effect and its influence on air temperature: a case study of Tarim Basin, Northwest China. J. Arid Land 8, 172–183.
Hao, X., Li, W., Deng, H., 2016. The oasis effect and summer temperature rise in arid regions - case study in Tarim Basin. Sci. Rep. 6, 35418.
HiWATER: Dataset of Hydrometeorological observation network, 2013. Cold and Arid Regions Science Data Center at Lanzhou. World Data System. http://card.westgis.ac.cn/hiwater/hmon.
Huang, J., Yu, H., Guan, X., Wang, G., Guo, R., 2016. Accelerated dryland expansion under climate change. Nat. Clim. Change 6 (2), 166–171.
Huang, J., Yu, H., Dai, A., Wei, Y., Kang, L., 2017. Drylands face potential threat under 2 °C global warming target. Nat. Clim. Change 7, 417–422.
Jiang, L., Ma, E., Deng, X., 2014. Impacts of irrigation on the heat fluxes and near-surface temperature in an inland irrigation area of northern China. Energies 7 (3), 1300–1317.
Kai, K., Matsuda, M., Sato, R., 1997. Oasis effect observed at Zhangye oasis in the Hexi corridor, China. J. Meteorol. Soc. Jpn 75, 1171–1178.
Kang, S., Eltahir, E.A.B., 2018. North China Plain threatened by deadly heatwaves due to climate change and irrigation. Nat. Commun. 9 (1), 1–9.
Kueppers, L.M., Snyder, M.A., Sloan, L.C., 2007. Irrigation cooling effect: regional climate forcing by land-use change. Geophys. Res. Lett. 34 (3).
Lee, X., Goulden, M.L., Hollinger, D.Y., Barr, A., Black, T.A., Bohrer, G., et al., 2011. Observed increase in local cooling effect of deforestation at higher latitudes. Nature 479, 384–387.
Li, X., Cheng, G., Liu, S., Xiao, Q., Ma, M., Jin, R., et al., 2013. Heihe watershed allied Telemetry experimental research (HiWATER): scientific objectives and experimental design. Bull. Am. Meteorol. Soc. 94, 1145–1160.
Li, X., Yang, K., Zhou, Y., 2016. Progress in the study of oasis-desert interactions. Agric. For. Meteorol. 230–231, 1–7.
Liu, S., Liu, H., Hu, Y., Zhang, C., Liang, F., Wang, J., 2007. Numerical simulations of land surface physical processes and land-atmosphere interactions over oasis-desert/Gobi region. Sci. China Earth Sci. 50, 290–295.
Liu, S.M., Xu, Z.W., Wang, W.Z., Jia, Z.Z., Zhu, M.J., Bai, J., Wang, J.M., 2011. A comparison of eddy-covariance and large aperture scintillometer measurements with respect to the energy balance closure problem. Hydrol. Earth Syst. Sci. 15, 1291–1306.
Liu, S.M., Li, X., Xu, Z.W., Che, T., Xiao, Q., Ma, M.G., Liu, Q.H., Jin, R., Ren, Z.G., 2018. The Heihe Integrated Observatory Network: a basin-scale land surface processes observatory in China. Vadose Zone J. 17.
Lobell, D.B., Bala, G., Bonfils, C., Duffy, P.B., 2006. Potential bias of model projected greenhouse warming in irrigated regions. Geophys. Res. Lett. 33.
Mahmood, R., Hubbard, K.G., Carlson, C., 2004. Modification of growing-season surface temperature records in the northern great plains due to land-use transformation: verification of modelling results and implication for global climate change. Int. J. Climatol. 24 (3), 311–327.
Micklin, P.P., 1988. Desiccation of the Aral sea: a water management disaster in the Soviet Union. Science 241, 1170–1176.
Nicholson, S.E., 2015. Evolution and current state of our understanding of the role played in the climate system by land surface processes in semi-arid regions. Global Planet. Change 133, 201–222.
Potchter, O., Goldman, D., Kadish, D., Iluz, D., 2008. The oasis effect in an extremely hot and arid climate: the case of southern Israel. J. Arid Environ. 72, 1721–1733.
Song, L., Kustas, W.P., Liu, S., Colaizzi, P.D., Nieto, H., Xu, Z., Ma, Y., Li, M., Xu, T., Agam, N., Tolk, J.A., Evett, S.R., 2016. Applications of a thermal-based two-source energy balance model using Priestley-Taylor approach for surface temperature partitioning under advective conditions. J. Hydrol. 540, 574–587.
Sun, L., Shen, B., Gao, Z., Sui, B., Bai, L., Wang, S.H., An, G., Li, J., 2007. The impacts of moisture transport of east Asian monsoon on summer precipitation in northeast China. Adv. Atmos. Sci. 24, 606–618.
Suyker, A.E., Verma, S.B., 2008. Interannual water vapor and energy exchange in an irrigated maize-based agroecosystem. Agric. For. Meteorol. 148, 417–427.
Taha, H., Akbari, H., Rosenfeld, A., 1991. Heat island and oasis effects of vegetative canopies: micro-meteorological field-measurements. Theor. Appl. Climatol. 44, 123–138.
Wang, X., Yang, H., Shi, M., Zhou, D., Zhang, Z., 2015. Managing stakeholders' conflicts for water reallocation from agriculture to industry in the Heihe River Basin in Northwest China. Sci. Total Environ. 505, 823–832.
Wang, L., Lee, X., Schultz, N., Chen, S., Wei, Z., Fu, C., Gao, Y., Yang, Y., Lin, G., 2018. Response of surface temperature to afforestation in the Kubuqi desert, inner Mongolia. J. Geophys. Res.: Atmospheres 128, 948–964.
Xiao, S., Xiao, H., Kobayashi, O., Liu, P., 2007. Dendroclimatological investigations of sea Buckthorn (Hippophae rhamnoides) and reconstruction of the equilibrium line altitude of the July first glacier in the western Qilian mountains, northwestern China. Tree-Ring Res. 63, 15–26.
Xu, H., Sui, L., Yuhong, L., Zhang, D., 2014. The Role of Water Users Associations in Integrated Water Resource Management of Zhangye City in Heihe River Basin, China.
Xu, Z.W., Ma, Y.F., Liu, S.M., Shi, S.J., Wang, J.M., 2017. Assessment of the energy balance closure under advective conditions and its impact using remote sensing data. J. Appl. Meteorol. Climatol. 56 (1), 127–140.
Yukie, H., Otto, S., 2011. Desertification: a Visual Synthesis. Unied Nations Convention to Combat Desertification (UNCCD).
Zhao, L., Lee, X., Smith, R.B., Oleson, K., 2014. Strong contributions of local background climate to urban heat islands. Nature 511, 216–219.
Zhao, L., Lee, X., Suyker, A.E., Wen, X., 2016. Influence of leaf area index on the radiometric resistance to heat transfer. Boundary-Layer Meteorol. 158, 105–123.
Zhou, Y., Li, X., 2019. Energy balance closures in diverse ecosystems of an endorheic river basin. Agric. Forest Meteorol. 274 118-13.